

# Defining high enthalpy geothermal drilling target with multi-physics integrated exploration program. Mayotte's Petite-Terre Island case study

A. Stopin, C. Dezayes and T. Farlotti

---

## Introduction

Mayotte is a volcanic island located on the ocean floor of the southern Somali Basin, between Africa and Madagascar, and is part of the Comoros Archipelago (Figure 9.1). The island is mainly composed of volcanic formations and is surrounded by the largest closed lagoon in the Indian Ocean, bordered by a coral reef barrier.

In 2017, Mayotte's electricity mix comprised 5% photovoltaic production distributed across more than 70 installations on the island, with the remaining 95% generated through diesel thermal power plants operated by Électricité de Mayotte. To diversify its electricity supply, the Departmental Collectivity of Mayotte implemented a comprehensive program aimed at leveraging renewable energy sources. As part of this initiative, the potential for geothermal energy production on the island was evaluated.



Figure 9.1 Location of Mayotte Island.

The French Geological Survey (BRGM), on behalf of and co-financed by the Departmental Collectivity of Mayotte, conducted a two-phase study titled “Assessment of Mayotte’s Geothermal Potential”. The first phase, conducted between 2005 and 2006, aimed to identify areas on the island with potential geothermal resources for electricity production. Results and main conclusions are detailed in the report by Traineau et al. (2006).

Petite-Terre was identified as a promising area despite the absence of direct evidence of geothermal resources. This selection was based on the island’s recent volcanism (<0.5 Ma), its unusual configuration for geothermal exploration, and the discovery of a significant magmatic CO<sub>2</sub> degassing zone east of the airport (Traineau et al., 2006).

The second phase of the study (2007-2008) focused on Petite-Terre, specifically the CO<sub>2</sub> degassing zone near the airport and the Dziani Dzaha Lake area, previously noted for gaseous emissions. Geophysical surveys (gravity, magnetism, and electrical resistivity) were conducted to detect potential heat sources such as hypovolcanic intrusions or magmatic chambers, as well as the presence of a hydrothermal system. Key results are presented in Pajot et al. (2007).

Based on the findings, including evidence of a dense and magnetic shallow body beneath the CO<sub>2</sub> degassing zone near the airport, a second stage of the study extended the resistivity surveys southward for deeper investigation. This stage also refined geochemical characterizations and natural gas flux measurements. The results, documented by Sanjuan et al. (2008), ruled out the presence of geothermal resources within the first 1000 m of depth and deemed it unlikely up to 1500 m – depths considered economically viable for electricity production.

However, given Petite-Terre's recent volcanism and its geological, geochemical, and geophysical context, the presence of a thermal anomaly or hydrothermal system at greater depths could not be excluded.

To confirm the existence and location of deeper geothermal resources, a comprehensive exploration program, including exploratory drilling, is required. Recognizing the cost and complexity of such an undertaking, Darnet et al. (2019) analyzed previous studies to evaluate the five elements of an active geothermal system (Figure 9.2):

1. heat source presence,
2. a cap rock preventing fluid escape,
3. a sustainable water recharge system,
4. a permeable medium (e.g. fractures),
5. the hydrothermal system's age.

Their analysis indicated a likelihood greater than 50% of finding an active geothermal system, though additional data were necessary. A customized exploration program was therefore defined, incorporating various methods to evaluate parameters such as temperature, volume, porosity, and permeability. Key components included:

- Geological data acquisition to analyze rock permeability and fracturing.
- Geochemical studies, including gas geothermometry, to estimate source temperatures.
- New onshore and offshore magnetotelluric (MT) surveys for 3D imaging of subsurface conductivity.
- Integration of data into GeoModeller™ (Lajaunie et al., 1997; Calcagno et al., 2008) to create a consistent 3D geological model.
- Hydrothermal simulations using the ComPASS (Lopez et al., 2018) platform to locate the optimal exploratory well site.

Dezayes et al. (2023) followed the exploration program described above. This chapter will focus on how the various geophysical methods of the program were used to define the geothermal drilling targets on Petite-Terre.

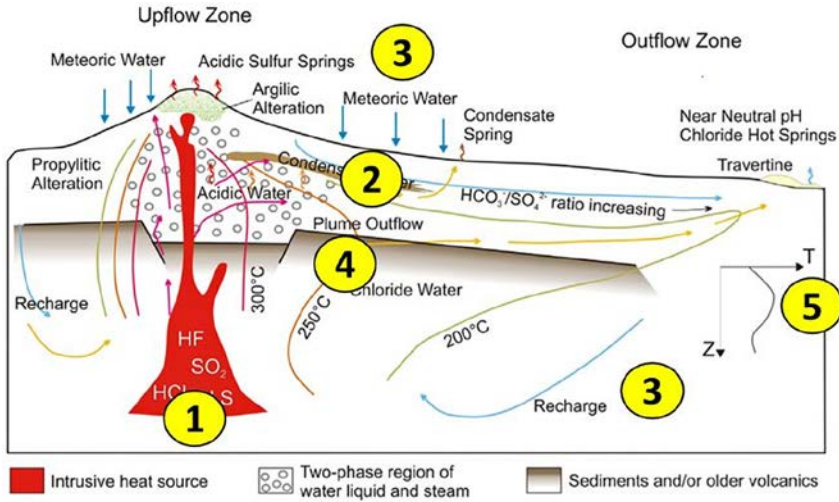


Figure 9.2 Constitutive elements of a volcanic hydrothermal system (Darnet et al., 2019).

## 9.1 Integration of magnetotelluric data

A total of 32 MT stations acquired during different periods (Darnet et al. 2019; Dezayes et al. 2023) are available. This dataset includes land MT stations and, for the first time, marine MT stations around the island, providing a more comprehensive image of the geological structures.

These 32 stations were inverted using the MININ3D code (Hautot et al., 2000, 2007) to create a 3D resistivity model. The results show a conductive structure overlying a resistive body, with a varying depth interface: 600 m below Moya Beach and 1.6 km below the airport (Figure 9.3). The model shares similarities with Pellerin et al. (1992) but reveals a more complex geometry. This interface can be interpreted as the boundary between a geothermal reservoir and its caprock.

In the map view at a depth of 2432 m, the resistive body displays a NW-SE global trend (Figure 9.3). The high quality of the hybrid land and sea MT measurements enabled the construction of a well-constrained 3D image of a potential geothermal target.

The 3D resistivity cube is interpreted based on the cross-sections shown in Figure 9.4. These cross-sections reveal a large, highly resistive volume compared to the surrounding host rock, with values ranging between 30 and 60 Ω·m (Figure 9.5). Based on the reference model, this zone corresponds to the reservoir altered by geothermal fluid circulation. Its boundaries can thus be delineated across all the cross-sections.

Above the reservoir lies the caprock, characterized by lower resistivity values, below 10 Ω·m. On the profiles, this zone is challenging to identify clearly due

to low resolution and likely interference from seawater infiltration at the surface. Nevertheless, a resistivity contrast can be observed between the upper part of the basement and the lower part, where resistivity is slightly higher. This boundary is marked as a dark red line in Figure 9.5.

It thus represents the basal boundary of a portion of the basement that may be partially clay-altered due to hydrothermal alteration, with its deepest levels likely containing the caprock.

Finally, very low resistivity values, again below  $10 \Omega\cdot\text{m}$ , are obtained at the bottom of the grid, towards the east. When placing this in the context of the reference conceptual model, it could correspond to the heat source of the geothermal system, located at around 12 km depth. Its roof is interpreted in the cross-sections (Figure 9.5), although the large depth introduces considerable uncertainty regarding its geometry.

This interpretation work allows for the construction of a 3D model that includes the three main elements of the geothermal system (Figure 9.6).

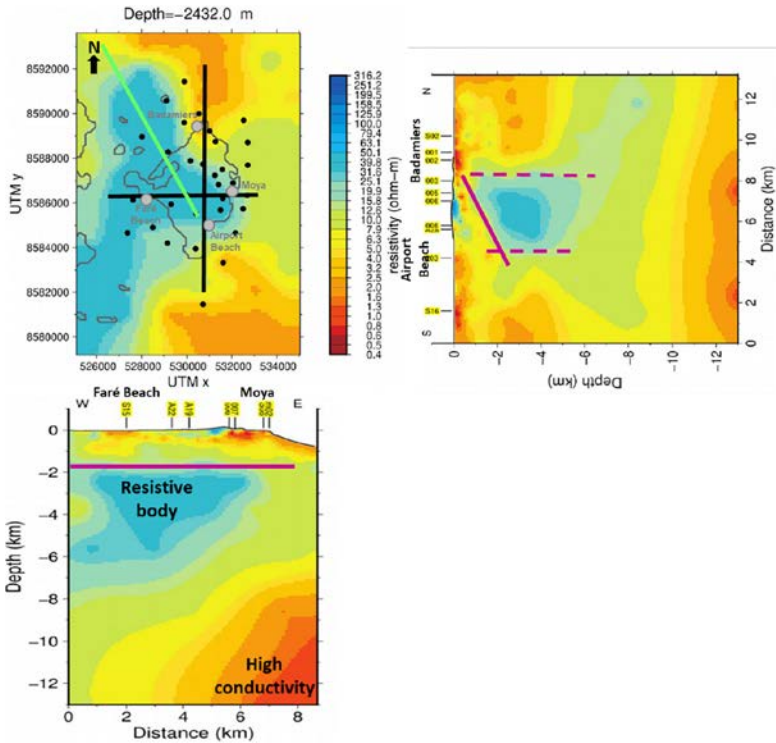


Figure 9.3 Resistivity map and cross-section on Petite Terre Island. On the map, black points: station location, black lines: location of cross-section, green line: SW-SE trend tendency. On cross-section, purple lines: limitation of resistive body.

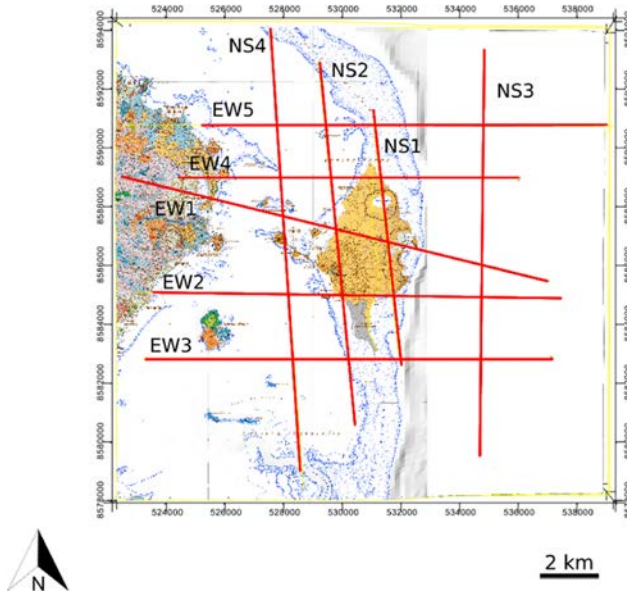


Figure 9.4 Location of the different cross-sections used to trace the boundaries of the formations. EW1 presents an oblique direction to match the conceptual WNW-ESE cross-section from Traineau et al. (2006), which has been integrated into the model.

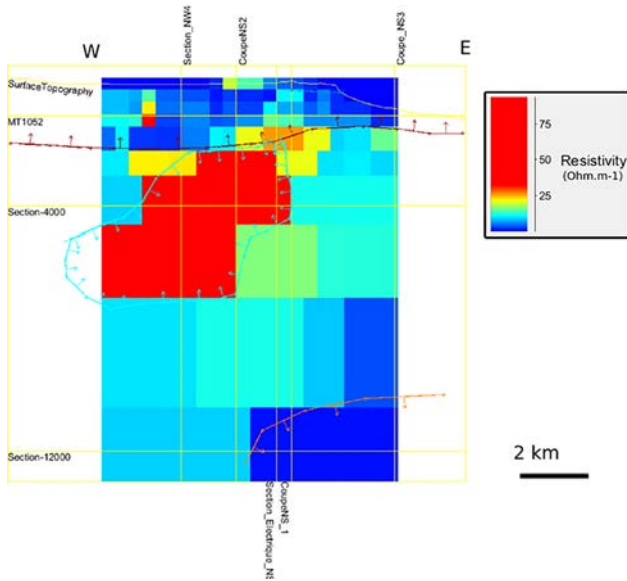


Figure 9.5 Example of interpretation of the EW1 cross-section from the resistivity grid. The drawn lines represent the bases of the formations. Dark red line: substrate, cyan line: reservoir, orange line: heat source.

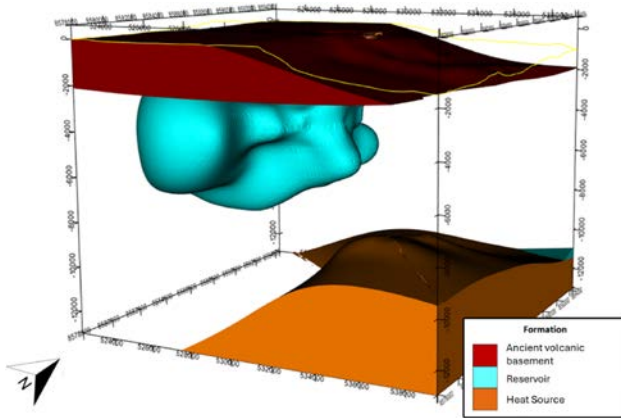


Figure 9.6 First model obtained considering only the results of MT data inversion.

Furthermore, on the field, the following surface manifestations have been observed:

- CO<sub>2</sub> degassing at the airport beach;
- CO<sub>2</sub> upwelling in a well in the center of the island.

These observations indicate the likely existence of a permeable zone passing through these two points, forming a N150°E direction. This is the main direction observed on the island outcrops and also corresponds to the regional geodynamic direction (Famin et al., 2020).

These elements lead to the presence of a possible sub-vertical fault passing through these points, defining a northeast boundary to the reservoir in the subsurface (Figure 9.7).

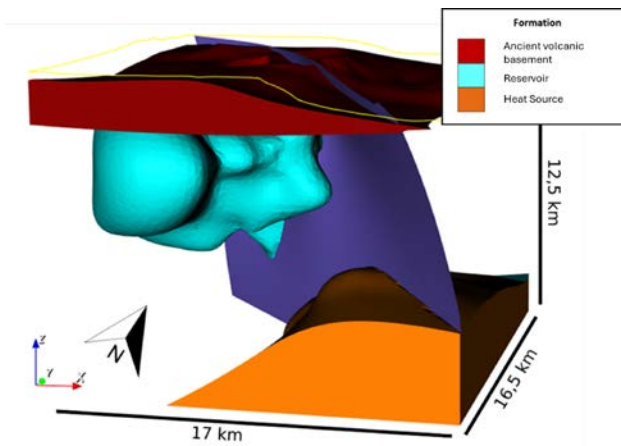


Figure 9.7 First model, with a N150°E fault based on the field observation. The confidence on the existence of this fault is very low at this stage of the model construction.

## 9.2 Electric profile integration

To better define the model at the surface, geophysical data probing shallower depths can be used. The electrical profile crossing the island from one end to the other (Figure 9.8) was carried out during the first geophysical campaign (Pajot et al., 2007) and then supplemented by a second series of acquisitions (Sanjuan et al., 2008).



Figure 9.8 Localisation of the electric profile (Sanjuan et al., 2008).

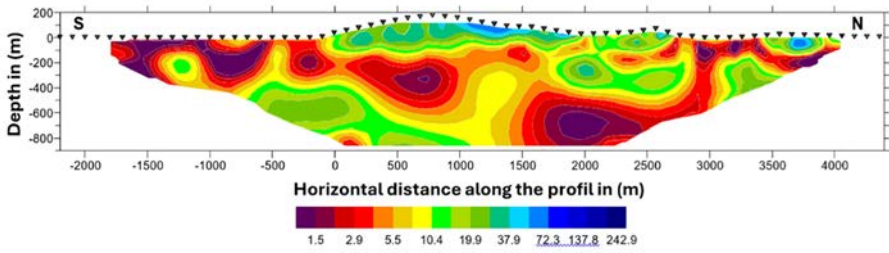


Figure 9.9 Resistivity ( $\Omega/m$ ) profile obtained from the inversion of the electric profile (Pajot et al., 2007).

A first interpretation had already been made of the resistivity profile obtained by inversion (Figure 9.9), but it was not complete enough to be integrated as is into the model. In light of the recent data, a new interpretation (Figure 9.10) is proposed, taking into account the identified formations.

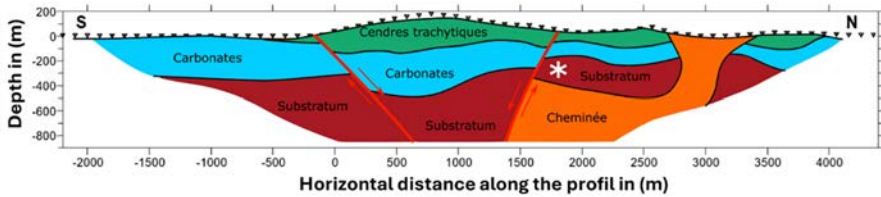
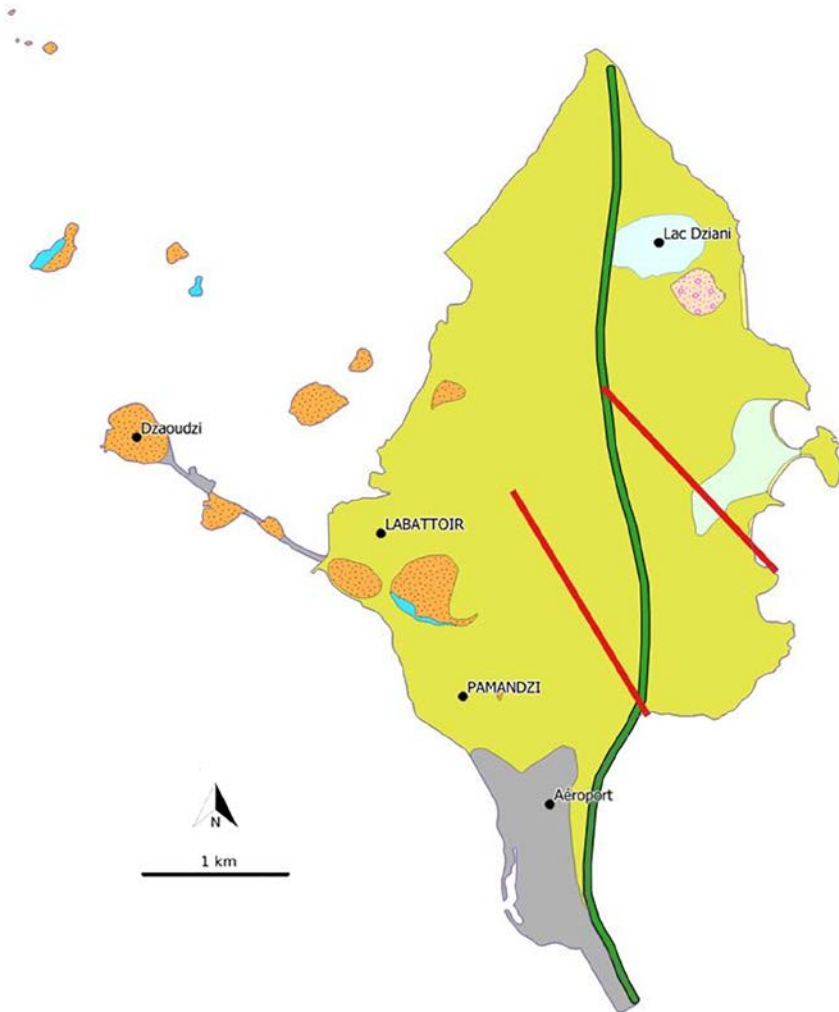


Figure 9.10 New interpretation of the electric profile.

This interpretation aligns with the overall architecture of Petite Terre, where volcanic material cuts through the carbonates, settling on top to form the island. The upper part is therefore composed of resistive trachytic ash and tuff. Below, the carbonated platform is conductive due to the intense water circulation and, in particular, saline intrusions that lower resistivity values. The Dziani lake area shows low resistivity, which extends clearly in depth. However, Dziani Lake is a maar created by phreatomagmatism. Therefore, it is reasonable to think that this low-resistivity zone is a conduit for fluid circulation. A zone of low resistivity, which could be linked to a high permeability zone, could, on the one hand, explain the magma upwelling and, on the other hand, the subsequent water circulation that causes hydrothermalism, leading to the alteration of magmatic rocks and thus low resistivity.

On the profile, two faults can be interpreted. The first to the south aligns with the one previously interpreted from the field data. This provides additional evidence for its presence, which was previously only inferred from gas emissions. The second interpreted fault dips southwest and forms a small graben in the middle of Petite Terre. To trace this fault on the map, however, another anchor point is needed.

During one of the early field campaigns (Traineau et al., 2006), a water seepage point was observed at the tip of one of the coves on Moya beach (Figure 9.11). However, a landslide made the area inaccessible, so the second field campaign in 2021 was unable to confirm and better define this zone. Nevertheless, considering that it is the same fault zone as the one defined on the section (Figure 9.10), its N140° direction appears consistent with the one to the south and with the geodynamic context (Famin et al., 2020; Figure 9.10). Confidence in this structure remains relatively low, however.



**Figure 9.11** Location of vertical permeability indicators used to trace the two faults. The red points indicate the locations of the faults on the electrical profile.

These points provide an orientation for the faults. To model them in GeoModeller, the software requires a dip value. Based on the apparent dips observed in the section (Figure 9.10) and the angle assumed relative to the fault azimuth, obtained from surface observation points (Figure 9.11), it is possible to assign a real dip to the model before creating 3D surfaces (Figure 9.12).

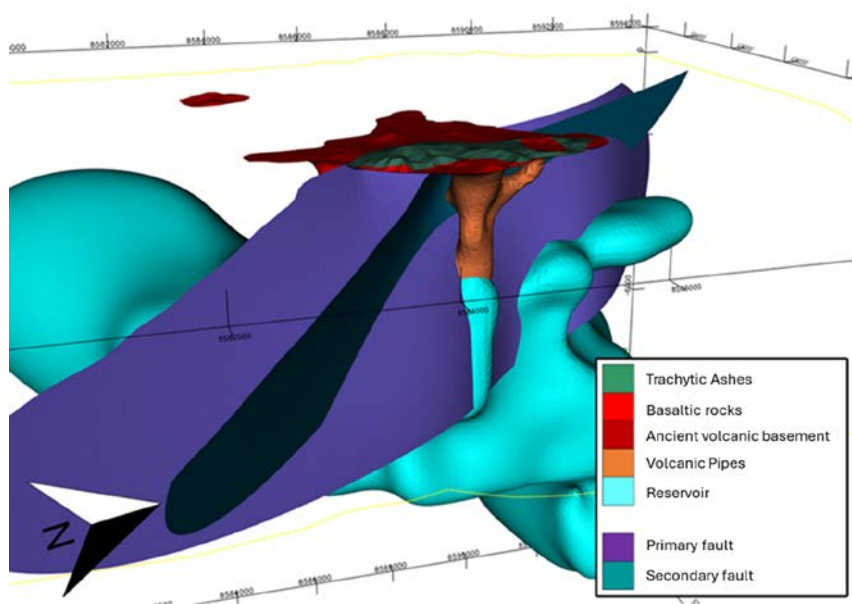


Figure 9.12 *The two normal faults modelled under Petite Terre.*

### 9.3 Gravimetric data integration

A total of 116 gravimetric measurement points acquired during the Pajot et al. (2007) campaign were inverted to obtain a density model. The inversion is performed jointly with the inversion of MT data, using a global correlation of resistivity and density structures as a constraint.

The density structure results (Figure 9.13) show a negative anomaly at the surface between the two interpreted faults forming a small graben. The main direction remains the same as the one observed in the previous paragraph, providing additional evidence supporting the presence of these faults, which were not visible in the resistivity inversion.

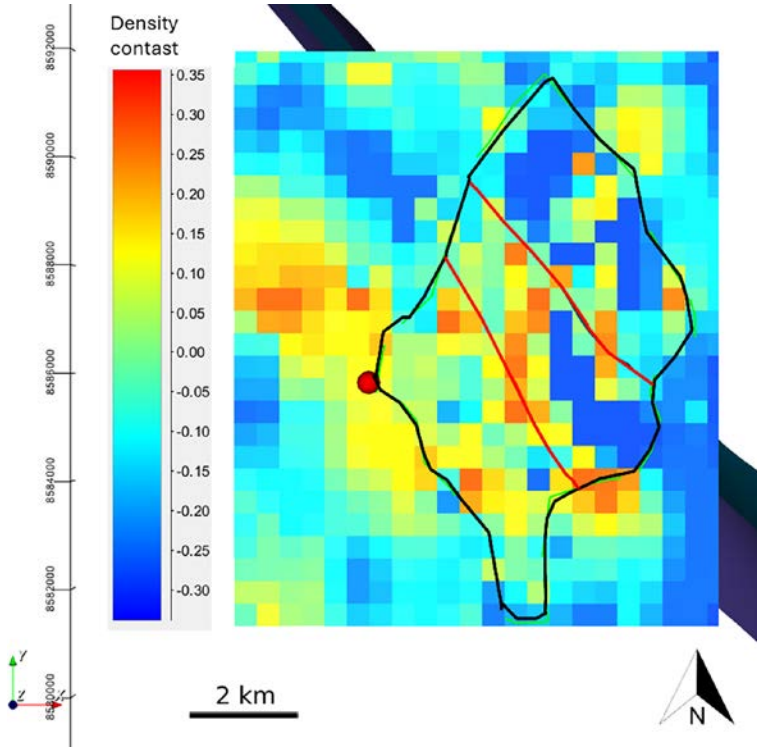


Figure 9.13 Surface density grid, with the outline of Petite Terre in black and the trace of the faults in red. A negative anomaly is observed between the two faults, which may indicate a collapse zone.

## 9.4 Final model

Geophysical data allowed for the placement of a reservoir, a heat source, the base of the volcanic substratum, as well as a number of areas with higher vertical permeability (chimneys) connecting the reservoir to surface material ejection zones. These areas likely correspond to relatively fractured environments, with the two major craters, Lac Dziani and La Vigie, being aligned along the main deformation direction of N150°E. The electrical profile also helped differentiate the volcanic rocks, distinguishing denser basalt-like rocks from the resistive trachytic ashes found around the maars.

The combination of all the data was used to position, with varying degrees of confidence, two N150°E-oriented faults, with the southernmost one being relatively certain, while uncertainties remain regarding the northern one. Following these

interpretation steps, the model underwent a phase of global consistency, during which many modifications were made to better align with reality. Among these, a final chimney was added in the southern part of the island to explain a high value observed in the magnetotelluric data at this location, which also correlates with visible scoria ejections on the surface (Figure 9.14).

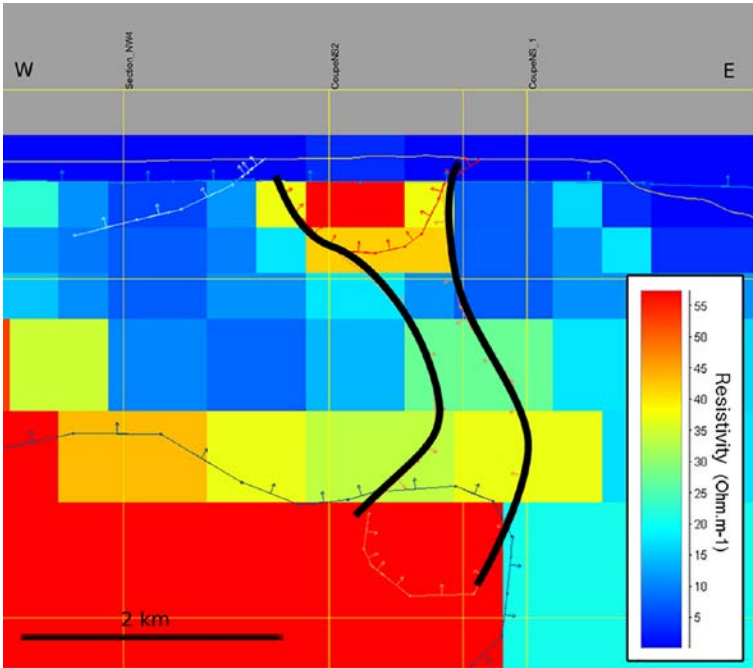


Figure 9.14 EW2 cross-section (see Figure 9.4) highlighting a potential material upwelling zone. The orange lines mark the boundaries of this “chimney”.

The geological model is then ready (Figure 9.15). It is consistent with the surface geological map and respects the general geometries observed. Some simplifications were made, notably the choice to assimilate the entire portion of Grande Terre within the model to volcanic substratum, even though in reality the area is covered by more recent minor lava flows. Since the project focuses primarily on Petite Terre, approximations at the edge of the model are not of major importance. The same applies to the geometry of the reservoir, which is, of course, largely extrapolated where data is absent.

With the finalized 3D geological model, the next step is to create a hydrothermal model. This stage helps determine the heat flow behaviours based on the geometry created, in order to estimate the most favorable region for the location of an initial exploration well.

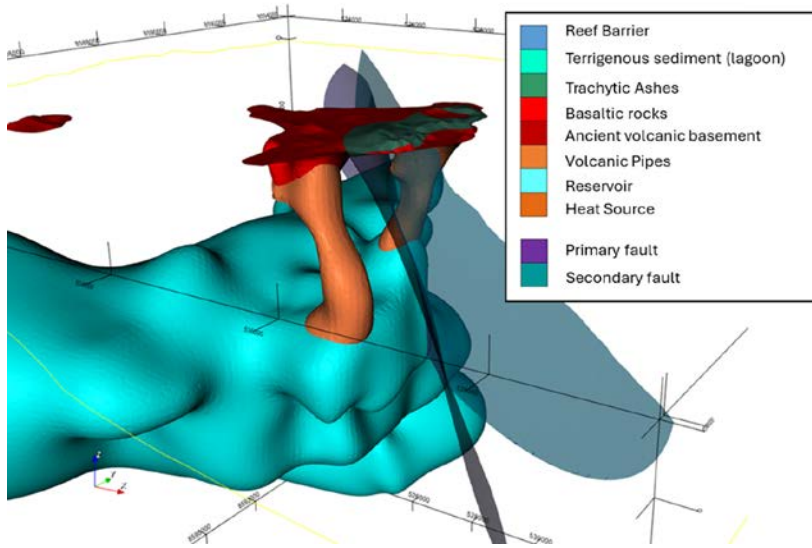
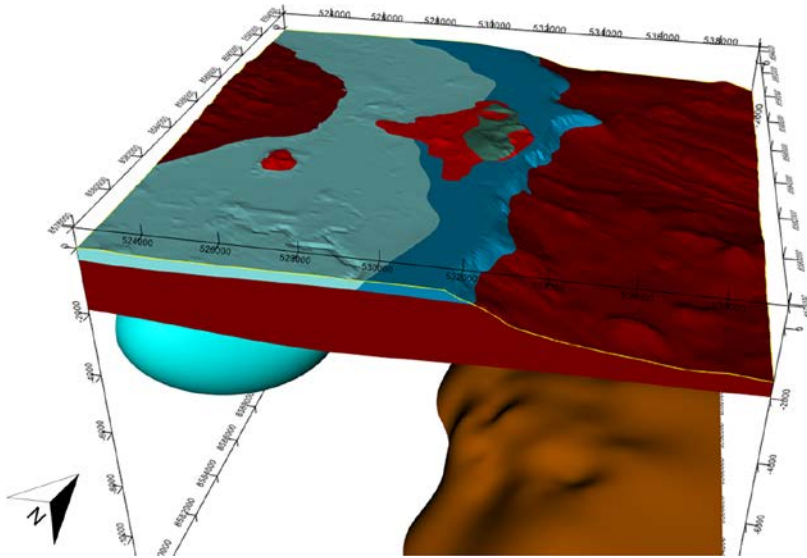
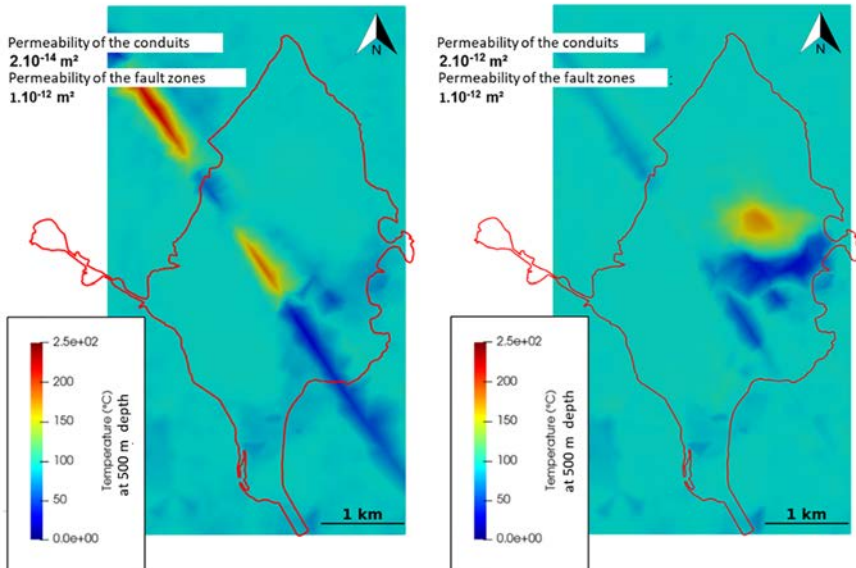


Figure 9.15 Final model. In the second image, the substrate and the more superficial parts have been masked for a better view of the faults and chimneys.

## 9.5 Choice of the drilling target

Based on the created geological model, the conceptual model defines the hydrothermal behavior of the system. The deep high conductivity zone constitutes the heat source. The resistive body forms the geothermal reservoir with a permeability higher than that of the surrounding basaltic rocks, while the upper high conductivity zone represents the impermeable caprock. Faults and conduits could channel deep geothermal fluid near the surface and have also been taken into account with higher permeability. A parametric study was conducted by varying the permeabilities of the different objects (conduits, faults, coral barrier) as well as the heat flow. The results of the various simulations show an upward movement of hot fluid at the center of the island, controlled by the volcanic conduit or the main fault, depending on the scenarios considered (Figure 9.16).



**Figure 9.16** Results of the numerical simulations for two scenarios. On the left, the permeability of the magma conduits is two orders of magnitude lower than the permeability of the fault zones. On the right, the permeability of the conduits and faults is equivalent.

In addition, a data assimilation study highlighted areas favorable to the presence of an underlying reservoir. This study, along with the results of numerical simulations, points to a central area of the island, between the Moya and Dziani maars, which could be a target for deep geothermal exploitation.

This work has encouraged industry players to submit an Exploration and Research Permit (PER) and to initiate more focused studies and consider an exploration drilling in the near future in the central area of the island. Integration of multi-physics geophysical data was key to obtain these results.

## References

- Calcagno P., Chiles J.P., Courrioux G., Guillen A. (2008) Geological modelling from field data and geological knowledge, *Phys. Earth Planet. Inter.* 171, 147-157, <https://doi.org/10.1016/j.pepi.2008.06.013>.
- Darnet M., Dezayes C., Sanjuan B., Tronel F., Traineau H. (2019) Étude de définition d'un programme d'exploration du potentiel géothermique profond à Petite Terre. Rapport final, BRGM/RP-69398-FR, 72 p., 36 fig., 9 tabl., 1 ann.
- Dezayes C., Stopin A., Wawrzyniak P., Gal F., Farlotti T., Les Landes A., Calcagno P., Traineau H., Hirsinger L., Macedo Serrano E., Chassagne R. (2023) Exploration des potentielles ressources géothermiques profondes de Petite Terre (Mayotte), Rapport final. BRGM/RP-72283-FR, 196 p., 107 fig., 19 tabl., 3 ann.
- Famin V., Michon L., Bourhane A. (2020) The Comoros archipelago: a right-lateral transform boundary between the Somalia and Lwandle plates, *Tectonophysics* 789, 228539, <https://doi.org/10.1016/j.tecto.2020.228539>.
- Hautot S., Single R., Watson J., Harrop N., Jerram D., Tarits P., Whaler K., Dawes D. (2007) 3-D magnetotelluric inversion and model validation with gravity data for the investigation of flood basalts and associated volcanic rifted margins, *Geophys. J. Int.* 170, 1418-1430.
- Hautot S., Tarits P., Whaler K., Le Gall B., Tiercelin J.J., Le Turdu C. (2000) Deep structure of the baringo rift basin (Central Kenya) from three-dimensional magnetotelluric imaging: Implications for rift evolution, *Journal of Geophysical Research: Solid Earth* 105, 23493-23518.
- Lajaunie C., Courrioux G., Manuel L. (1997) Foliation fields and 3D cartography in geology: Principles of a method based on potential interpolation, *Mathematical Geology* 29(4), 571-584.
- Lopez S., et al. (2018) Geothermal Modeling in Complex Geological Systems with the COMPASS Code. Stanford, United States, Stanford Geothermal Workshop 2018 - 43rd Workshop on Geothermal Reservoir Engineering.
- Pajot G., Debeglia N., Miéché J.-M. (2007) Estimation du potentiel géothermique de Mayotte: Phase 2 - Étape 1, Investigations géophysiques par gravimétrie, magnétisme et panneau de résistivité électrique, Rapport intermédiaire, BRGM/RP-56027-FR, 60 p.

- Pellerin L., Johnston J.M., Hohmann G.W. (1992) Evaluation of electromagnetic methods for geothermal exploration, *SEG Technical Program Expanded Abstracts* 1992, 405-408, <https://doi.org/10.1190/1.1822102>.
- Sanjuan B., Baltassat J.-M., Bezelgues S., Brach M., Girard J.-F., Mathieu F, avec la collaboration de Debeglia N., Dupont F, François B., Miehé J.-M., Pajot G., Traineau H. (2008) Estimation du potentiel géothermique de Mayotte: Phase 2 - Étape 2, Investigation géologiques, géochimiques et géophysiques complémentaires, synthèse des résultats, Rapport BRGM/RP-56802-FR, 82 p.
- Traineau H., Sanjuan B., Brach M., Audru J.-C. (2006) État des connaissances du potentiel géothermique de Mayotte, Rapport BRGM/RP-54700-FR, 81 p.